inorganics

MDPI

Article

Metal (Hg, Pt, Ru) Bisalkynyl Bridge between Tetrathiafulvalene Electrophores and Electronic Interplay

Morgan Auffray, Antoine Vacher, Thierry Roisnel and Dominique Lorcy *

Univ Rennes, CNRS, ISCR (Institut des Sciences Chimiques de Rennes)-UMR 6226, F-35000 Rennes, France; morgan.auffray@gmail.com (M.A.); antoine.vacher@univ-rennes1.fr (A.V.); thierry.roisnel@univ-rennes1.fr (T.R.)
* Correspondence: Dominique.lorcy@univ-rennes1.fr

Received: 30 March 2018; Accepted: 26 April 2018; Published: 1 May 2018

Abstract: A series of metal (Hg, Pt, Ru) bis(alkynyl-tetrathiafulvalene) complexes have been investigated to study the electronic interplay between the metal and the tetrathiafulvalene (TTF), as well as between the two peripheral TTF electrophores along the organometallic bridge. Cyclic voltammetry experiments, together with spectro-electrochemical investigations, have shown the electronic effect of the metal center through the linker on redox properties of the TTF, as well as the influence of the length of the conjugated organic linker. These data show that the degree of coupling can be modulated from no coupling with mercury to appreciable electronic coupling between different electrophores with ruthenium.

Keywords: tetrathiafulvalene; alkynyl complexes; ruthenium; platinum; mercury; electrochemistry; electronic interaction

1. Introduction

Tetrathiafulvalene (TTF) dimers have attracted attention in past decades as potential building blocks for the formation of mixed valence species, $(TTF_2)^{+\bullet}$ which is key for the elaboration of conducting materials in charge transfer salts [1–3]. Different organic spacer groups, conjugated or non-conjugated, have been used to connect the two TTF moieties and, depending on the nature of the spacer, either through space or through bond interactions, have been observed [1,4–9]. Organic spacer groups are not the only linkers which have been studied. Indeed, the grafting of functional groups on the TTF core allows the formation of TTF ligands. The coordination chemistry of two of these ligands towards the metallic center also generates various dimeric structures [10–12]. Most of the interactions detected through organic linkers are weak and coordination chemistry does not allow an increase of electronic interplay [13–15]. On the other hand, the use of an organometallic linker such as the *trans* bis(acetylide) ruthenium one in *trans*-$[Ru(C{\equiv}CMe_3TTF)_2(dppe)_2]$ mediates strong electronic coupling between the two TTFs [16]. Moreover, within this complex, the TTF and the ruthenium center are also strongly electronically coupled [17,18]. Other *trans* bis(acetylide) metallic linkers have also been reported in the literature (M = Cr [19–22], Pt [23]) but these organometallic linkers do not allow an electrochemically measurable electronic interaction between the TTFs. However, the absence of electrochemical evidence for the formation of mixed valence species in the case of the Cr bis(acetylide) linker did not impede on the formation of a mixed valence species in the solid state. In this context, we also focused on another metal center which, compared to Ru and Pt, has been poorly explored so far in TTF chemistry as a part of the organometallic linker, that is mercury [24]. Mercury(II) ion is known to form various complexes with acetylide ligands by forming two-coordinate d^{10} mercury(II) species [25–27]. Therefore, we investigated the synthesis of a complex where the mercury was linked

to two TTF units via such an alkynyl linkage and we describe here this bis(acetylide) mercury complex, *trans*-[Hg(C≡CMe_3TTF)$_2$] (Chart 1). We also recently reported the effect of the length of the conjugated linker between the TTF core and the Ru center by replacing the ethyne linker with a butadiyne rod [28]. This structural modification between the Ru and the two TTFs still allows for an electronic interplay between the three electrophores however, with weaker interactions, such as in the trimetallic complexes with ferrocene electrophore in *trans*-[Ru(C≡C–C≡CFc)$_2$(dppe)$_2$] vs. *trans*-[Ru(C≡CFc)$_2$(dppe)$_2$] [29]. Thus, it was of interest to prepare the two mononuclear complexes, the *trans*-[Hg(C≡C–C≡CMe_3TTF)$_2$] and the *trans*-[Pt(C≡C–C≡CMe_3TTF)$_2$(PPh_3)$_2$], to compare their electronic properties with those with a shorter spacer group, the metal bis(acetylide) complexes (Pt, Hg). Herein, we report the synthesis and the electronic properties of Hg, Pt and Ru complexes where two TTFs are linked to the metal through an ethynyl or a butadiyne linker, together with the complex where only one TTF is connected to the Ru center through a butadiyne rod (Chart 1). Electrochemical and spectroelectrochemical investigations were used to evidence, depending on the metal and the length of the linker between the metal and the electrophores, the electronic interplay between the various electrophores.

Chart 1

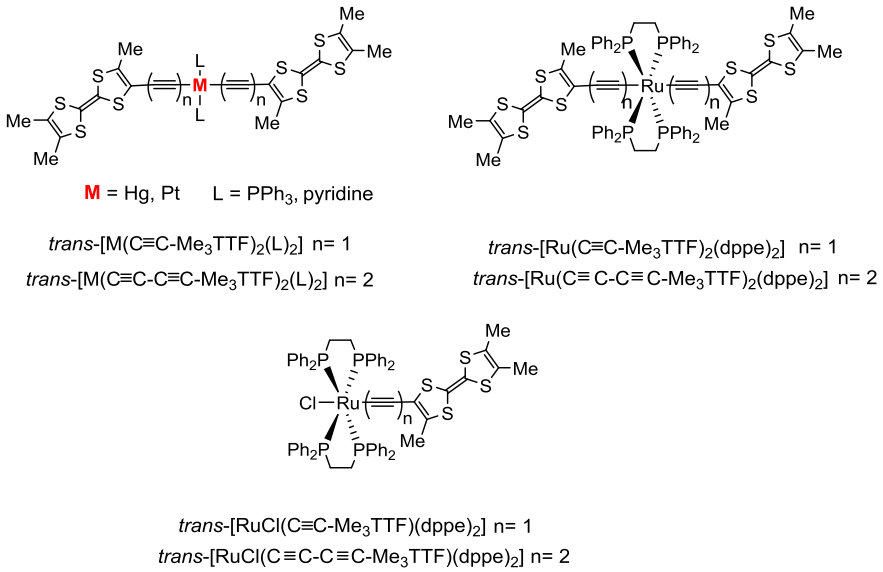

Chart 1. Metal (Hg, Pt, Ru) bis(alkynyl-tetrathiafulvalene) and mono substituted Ru complexes.

2. Results

The various complexes were synthesized, starting from either Me_3TTF-ethyne **3** [16–18] or Me_3TTF-buta-1,3-diyne **4** [30]. With regard to the Me_3TTF-buta-1,3-diyne **4**, we also used an alternative approach, starting from the trimethylsilylprotected TTF-ethyne **1**, which is the precursor to TTF **3**, according to the synthetic pathway described in Scheme 1 [31]. The extension of the chain was realized by successively adding potassium carbonate then trimethylsilylacetylene (TMSA) in the presence of CuI and tetramethylethylenediamine (TMEDA) in dichloromethane to a solution of TTF **1**. Using this strategy, the trimethylsilylprotected TTF-buta-1,3-diyne **2** was obtained together with an important quantity of 1,4-bis(trimethylsilyl)butadiyne. Desilylation of TTF **2** with KF in MeOH provided for Me_3TTF-buta-1,3-diyne TTF **4** in excellent yields.

Bis(TTF-alkynyl)mercury complexes **5** and **6** were prepared by reacting TTF **3** or **4** with [Hg(OAc)$_2$] in refluxing THF (Scheme 2) [32]. In both cases, a powder that is insoluble in usual organic solvents, was obtained. Nevertheless, an FTIR analysis of these powders demonstrated that the characteristic C–H stretching vibration band observed for the terminal alkynes at $\nu_{\equiv C-H}$ = 3306 cm^{-1} and 3278 cm^{-1} for **3** and **4** respectively had disappeared in the spectra of complexes **5** and **6**. Moreover, the stretching vibration band of the C≡C bonds in complex **5** was located at $\nu_{C\equiv C}$ = 2141 cm^{-1}, which was also

consistent with the stretching frequency observed in the analogous ferrocenyl derivative $Hg(C{\equiv}CFc)_2$ ($\nu_{C\equiv C}$ = 2141 cm^{-1}) [33]. However, in complex **6**, the vibration band was slightly shifted at $\nu_{C\equiv C}$ = 2151 cm^{-1}. Both $\nu_{C\equiv C}$ values were different from the ones observed in the starting TTF alkynes ($\nu_{C\equiv C}$ = 2190 cm^{-1} for **3** and 2201 cm^{-1} for **4**), confirming the formation of the mercury complexes. It is worth mentioning that we did not observe a decomposition of complexes **5** and **6** over time, even without purification, as was observed for the ferrocenyl complex $Hg(C{\equiv}CFc)_2$ [34]. In order to purify these complexes, we recrystallized them in pyridine. Single crystals were obtained for **5**, allowing an X-ray diffraction study.

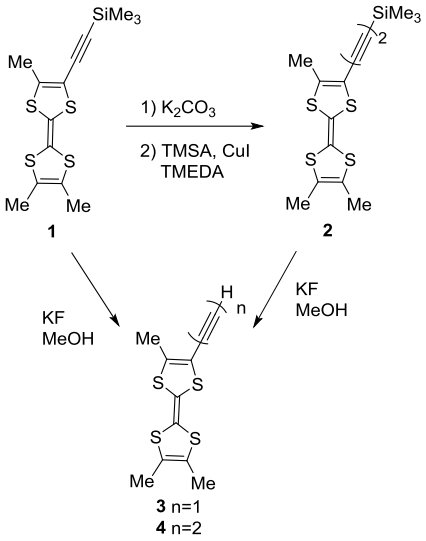

Scheme 1. Synthesis of the tetrathiafulvalene (TTF) precursors.

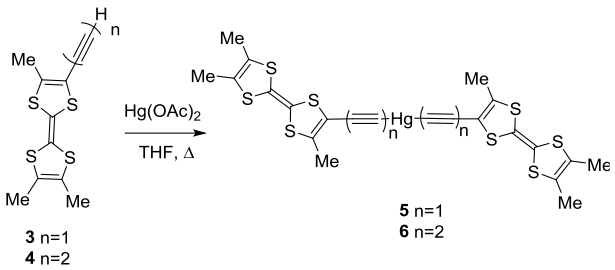

Scheme 2. Synthesis of mercury alkynyl complexes.

The molecular structure given in Figure 1 confirms the formation of the mercurial complex **5** and also indicates the presence of two pyridines in the coordination sphere of the Hg atom, leading to a four coordinate Hg atom with a square planar geometry. Within this complex, denoted *trans*-$[Hg(C{\equiv}CMe_3TTF)_2(pyr)_2]$, the TTF-acetylide are located in a *trans* arrangement around the Hg atom. For comparison purposes, we collected in Table 1 the bond lengths of the metal (M = Ru, Pt, and Hg) bis(alkynyl) linkers. The Hg–C and Hg–N distances amount to 2.032(6) and 2.850(6) Å respectively and the C≡C bond distance reaches 1.196(9) Å, i.e., slightly shorter than the one found in the ruthenium and the platinum complexes but longer than the starting Me_3TTF-alkyne (1.152(8) Å) (Table 1) [16]. The TTF units are non-planar and exhibit a boat conformation with the dithiole rings folded along the S···S axis with values of about 26° and 10° and a bond length of the central C=C bond consistent with the presence of neutral TTF (1.341 Å). The organometallic linker –C≡C–Hg–C≡C– between the two TTFs is close to linear, with C–Hg–C and Hg–C≡C angles of 176.9(5) and 179.9(2)° respectively.

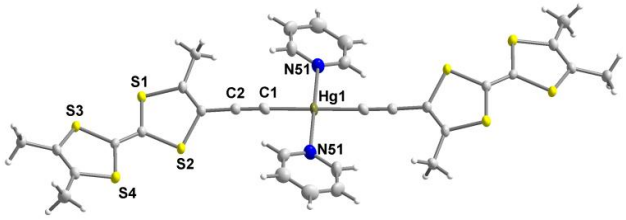

Figure 1. Molecular structure of *trans*-[Hg(C≡CMe_3TTF)$_2$(pyr)$_2$]. Ellipsoids are drawn at the 50% probability level.

Table 1. Selected bond distances of the acetylide linker in (Å) and C≡C stretching IR frequency ($\nu_{C\equiv C}$) in the metal bis(acetylide) complexes (Hg, Pt, Ru) together with TTFs **1** and **3**.

Me_3TTF—**a**—**b**—**c**—R

Compound	a	b	c	$\nu_{C\equiv C}$ (cm^{-1})	Ref.
TTF **1** (R = $SiMe_3$)	1.422(3)	1.209(3)	1.841(3)	2140	[16]
TTF **3** (R = H)	1.408(6)	1.152(8)	0.950(6)	2090	[16]
trans-[Pt(C≡CMe_3TTF)$_2$(PPh_3)$_2$]	1.422(6)	1.220(5)	1.999(5)	2086	[23]
trans-[Ru(C≡CMe_3TTF)$_2$(dppe)$_2$]	1.423(3)	1.203(3)	2.069(3)	2029	[16]
trans-[Hg(C≡CMe_3TTF)$_2$(Pyr)$_2$]	1.431(9)	1.196(9)	2.032(6)	2141	this work

The synthesis of the target platinum complex, *trans*-[Pt(C≡C–C≡CMe_3TTF)$_2$(PPh_3)$_2$] **7** was realized, starting from TTF-butadiyne **4** as reported in Scheme 3. The *cis*-Pt(PPh_3)$_2$$Cl_2$ complex in the presence of triethylamine and CuI in dry dichloromethane was reacted with two equivalents of TTF **4** to afford the *trans*-complex, *trans*-[Pt(C≡C–C≡CMe_3TTF)$_2$(PPh_3)$_2$] **7** [35]. The *trans* configuration was confirmed by the ^{31}P NMR spectrum of the complex, which only shows one signal at 18.1 ppm, indicating the equivalence of the two phosphorus atoms around the Pt(II) centre.

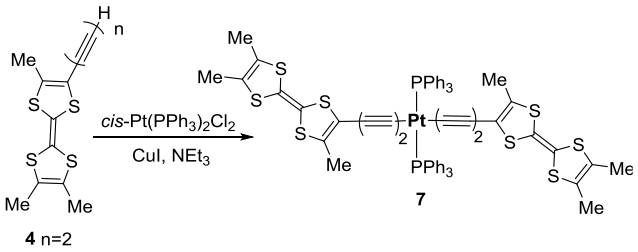

Scheme 3. Synthesis of *trans*-[Pt(C≡C–C≡C Me_3TTF)$_2$(PPh_3)$_2$].

Recently, we reported the synthesis of *trans*-[Ru(C≡C–C≡CMe_3TTF)$_2$(dppe)$_2$] **8** (dppe = $Ph_2PCH_2CH_2PPh_2$) [28] by simply reacting TTF **4** with half an equivalent of *cis*-[$RuCl_2$(dppe)$_2$] in the presence of $NaPF_6$ and triethylamine in dichloromethane at room temperature under inert atmosphere (Scheme 4). Interestingly, by using the same conditions but one equivalent of *cis*-[$RuCl_2$(dppe)$_2$], we synthesized the mononuclear ruthenium complex where the Ru is connected to only one TTF through a butadiyne bridge, *trans*-[RuCl(C≡C–)$_2$$Me_3$TTF(dppe)$_2$] **9** (Scheme 4). Monitoring the reaction by ^{31}P NMR spectroscopy shows that the signals of the starting complex *cis*-[$RuCl_2$(dppe)$_2$] at δ_p = 37.8 ppm and δ_p = 45.1 ppm gradually disappear in favor of a signal at δ_P = 47.9 ppm associated with the formation of the monosubsituted complex *trans*-[RuCl(C≡C–)$_2$$Me_3$TTF (dppe)$_2$] **9**. The single peak indicates the equivalence of the phosphorus atoms of the dppe ligands due to the *trans*-configuration.

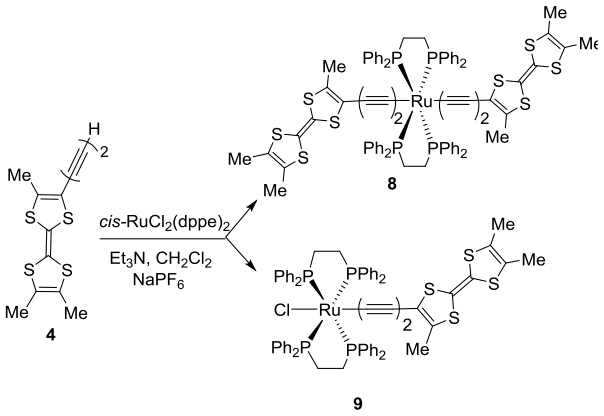

Scheme 4. Synthesis of the Ru complexes.

Crystals of the *trans*-[RuCl(C≡C–)$_2$Me$_3$TTF(dppe)$_2$] complex **9** were obtained by a slow diffusion of pentane into a concentrated solution of the complex in CH_2Cl_2 under inert atmosphere. This complex crystallizes in the triclinic system, space group $P\bar{1}$, with one independent molecule and two CH_2Cl_2 molecules. The molecular structure of **9** is shown in Figure 2. The Ru(II) atom is chelated by two dppe units in the equatorial plane and the octahedral coordination geometry is completed by a chloride ligand *trans* coordinated to the TTF-butadiyne. The neutral TTF unit (the central C=C bond length amounts to 1.306 Å) exhibits a boat conformation with the dithiole rings folded along the S···S axis with asymmetric folding angles of 6 and 14°. The –Ru–C≡C–C≡C– organometallic fragment is slightly bent, with angles at –C$_\alpha$≡C$_\beta$–C$_\gamma$, –C$_\beta$–C$_\gamma$≡C$_\delta$– and –C$_\gamma$≡C$_\delta$–C$_{TTF}$ of 170.32°, 166.84° and 178.25° respectively. It is interesting to compare the bond lengths of the butadiyne rod with those observed in the starting TTFs and the previously reported complex with two TTFs, namely *trans*-[Ru(–C≡C–C≡C–Me$_3$TTF)$_2$(dppe)$_2$], (Table 2) [28]. Within the mono-TTF substituted complex, the bond lengths for the butadiyne rod indicate a high degree of conjugation compared to the TTF precursors **2** and **4**. This higher degree of conjugation can also be visualized on the IR frequencies of the acetylide bonds as for the monosubstituted complex. They are found at a lower energy than in the starting TTFs **2** and **4** (Table 2). The Ru-Cα distance of 2.075(6) Å stands in the same range as other ruthenium *trans* coordinated alkyne ligand (Tables 1 and 2) [16,29,36].

The redox properties of the different complexes have been investigated by cyclic voltammetry. The redox potentials are collected in Table 3 together with those of the starting TTFs **3**–**4** and the previously reported Ru and Pt analogous complexes for comparison. Except for the mercury complexes, which were analyzed in DMF, all the other derivatives were investigated in CH_2Cl_2 using NBu_4PF_6 as a supporting electrolyte.

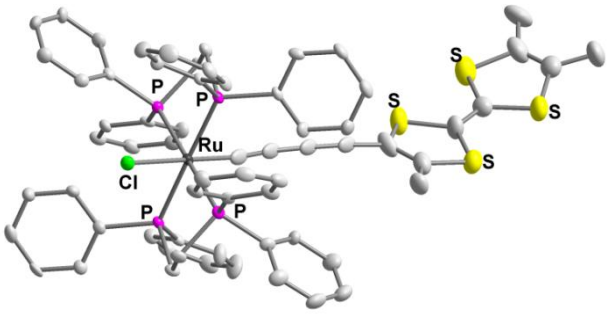

Figure 2. Molecular structure of *trans*-[RuCl(–C≡C)$_2$–Me$_3$TTF (dppe)$_2$] complex **9** (H atoms are omitted for clarity). Ellipsoids are drawn at the 50% probability level.

Table 2. Selected bond distances (Å) in the mono and bis TTF Ru complexes together with TTFs **2**, **4**.

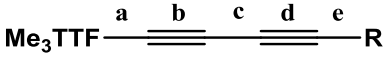

Compound	a	b	c	d	e	$\nu_{C\equiv C}$ (cm^{-1})	Ref.
TTF **2** (R = $SiMe_3$)	1.414(5)	1.205(5)	1.376(5)	1.208(5)	1.845(4)	2181, 2097	[30]
TTF **4** (R = H)	1.416(4)	1.199(4)	1.376(4)	1.177(4)	0.950(3)	2201	[30]
8 (R = Ru)	1.414(3)	1.215(3)	1.370(3)	1.218(3)	2.051(2)	2129, 1993	[28]
9 (R = Ru)	1.368(10)	1.272(9)	1.253(9)	1.202(9)	2.075(6)	2134, 2011	this work

Table 3. Redox potentials of the various complexes issued from TTFs **3** and **4** in CH_2Cl_2, E vs. SCE.

Compound	E_1 (TTF)	E_2 (TTF)	E_{ox} (Ru)	Ref.
TTF **3**	0.38 (0.47 [a])	0.88 (0.70 [a])	-	[17] ([a] this work)
TTF **4**	0.40 (0.50 [a])	0.90 (0.71 [a])	-	[30] ([a] this work)
trans-[Hg($C\equiv CMe_3TTF)_2$] **5**	0.43 [a]	0.67 [a]	-	this work
trans-[Hg($C\equiv CMe_3TTF)_2(pyr)_2$]	0.47 [a]	0.72 [a]	-	this work
trans-[Hg($(C\equiv C–)_2Me_3TTF)_2$] **6**	0.47	0.70	-	this work
trans-[Pt($C\equiv CMe_3TTF)_2(PPh_3)_2$]	0.21	0.72	-	[23]
trans-[Pt($(C\equiv C–)_2Me_3TTF)_2(PPh_3)_2$] **7**	0.33	0.83	-	this work
trans-[Ru($C\equiv CMe_3TTF)_2(dppe)_2$]	0.05/0.16	0.58/0.69	1.33	[16]
trans-[Ru($(C\equiv C–)_2Me_3TTF)_2(dppe)_2$] **8**	0.24	0.69/0.76	1.13	[28]
trans-[RuCl($C\equiv CMe_3TTF)(dppe)_2$]	0.07	0.52	1.07	[17]
trans-[RuCl($(C\equiv C–)_2Me_3TTF)(dppe)_2$] **9**	0.23	0.62	1.02	this work

[a] performed in DMF.

Among all the investigated complexes, only the Ru complexes display a redox process associated with the metal centre. All the other complexes exhibit two well defined reversible oxidation waves associated with the redox signature of the TTF cores (Figure 3). With regard to the Hg and Pt complexes, because these complexes include two TTFs, this indicates that either no interaction occurs via the organometallic linker between the two TTF cores or that these interactions are too weak to be observed at the cyclic voltammetry scale. Therefore, the two TTFs oxidize, essentially simultaneously, into the TTF cation radicals and then to the TTF dications. The crystalline complex *trans*-[Hg($C\equiv CMe_3TTF)_2(pyr)_2$] was also investigated in the same conditions as **5**. It is interesting to note that an anodic shift of about 40 mV is observed on the oxidation potentials of the TTFs when two pyridine ligands are coordinated to the mercury atom (Table 3). On the contrary, for the Ru bis(acetylide) complex, *trans*-[Ru($C\equiv CMe_3TTF)_2(dppe)_2$], each TTF is oxidized sequentially into a TTF radical cation and TTF dication. This indicates that the Ru bis(acetylide) linker is the only organometallic linker which allows the formation of mixed valence species ($TTF/TTF^{+\bullet}$ and $TTF^{+\bullet}/TTF^{2+}$) within the series [16]. On the other hand, the introduction of a Ru bis(butadiyne) spacer group does not allow the observation of electronic interplay on the first redox process between the two TTF cores but only on the second redox process [28]. This redox behavior is uncommon in the case of TTF dimers and could be tentatively assigned to electrostatic repulsion generated in the $TTF^{+\bullet}/TTF^{2+}$ species, as previously observed for the oxidation of the TTF moieties in their dicationic states for the *trans*-[Ru($C\equiv CMe_3TTF)_2(dppe)_2$] [16].

Another feature is the electronic effect of the metal center through the linker on the redox properties of the TTF. For instance, the presence of the mercury atom does not significantly modify the oxidation potentials of the TTF. This is reminiscent of what was observed in the case of the iron or chromium acetylide-TTF type complex, Cp*(dppe)FeC≡CTTFMe_3 [37,38] and [CrCyclam($C\equiv CEDTMeTTF)_2$]OTf [19–22]. In contrast, a cathodic shift of the redox potentials is observed when a platinum or a ruthenium atom is connected to the TTFs. Interestingly, the cathodic shift observed for the Ru complexes is more pronounced, indicating a large increase of the electron density of the Ru organometallic fragment on the TTF cores through the conjugated linker. It is worth mentioning that this electronic interaction between the ruthenium center and the TTFs is similar in the mono- and the bis-substituted complexes, *trans*-[RuCl($(C\equiv C–)_nMe_3TTF)(dppe)_2$]

and *trans*-[Ru((–C≡C)$_n$Me$_3$TTF)$_2$(dppe)$_2$] (n = 1, 2) respectively. For all the ruthenium complexes, the reversible oxidation of the ruthenium center is ascribed to the last redox process observed on the cyclic voltammogram (Figure 3b). The $Ru^{II/III}$ oxidation is anodically shifted compared to *cis*-$RuCl_2(dppe)_2$ (0.50 V vs. SCE) due to the presence of the dicationic TTF acting as an acceptor in the vicinity of Ru, confirming the electronic interaction between the organic and inorganic electrophores along the conjugated linker.

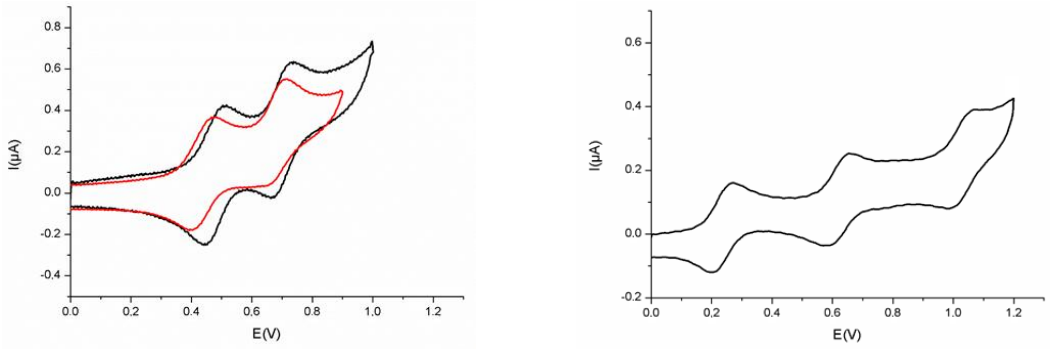

(**a**) (**b**)

Figure 3. CV of (**a**) *trans*-[Hg(C≡CMe$_3$TTF)$_2$] **5** (red curve) and *trans*-[Hg(C≡C–C≡CMe$_3$TTF)$_2$] **6** (black curve) in DMF, (**b**) *trans*-[RuCl(C≡C–C≡CMe$_3$TTF)(dppe)$_2$] **9** in CH_2Cl_2, with NBu_4PF_6 0.1 M, E vs. SCE.

If we concentrate now on the effect of the length of the conjugated organic linker between the TTF and the metal center, the additional acetylenic group modifies the electronic interplay between these two electrophores. Indeed, comparison of the redox potentials of the TTF within the different complexes obtained with Me$_3$TTF ethyne **3** and Me$_3$TTF butadiyne **4** (Table 3) highlights this influence as the cathodic shifts observed for the complexes with the diacetylenic rod are less pronounced than those with an acetylenic one. This result is in agreement with the work performed by Touchard et al. on *trans*-[Ru(C≡CFc)$_2$(dppe)$_2$] and *trans*-[Ru(C≡C–C≡CFc)$_2$(dppe)$_2$] [29].

UV–Vis-NIR spectroelectrochemical investigations were carried out on *trans*-[Hg(C≡CMe$_3$TTF)$_2$(dppe)$_2$] **5**, *trans*-[Pt(C≡C–C≡CMe$_3$TTF)$_2$(PPh$_3$)$_2$] **7** and *trans*-[RuCl(C≡C–C≡CMe$_3$TTF)(dppe)$_2$] **9** complexes. Due to the low solubility of the mercury complex **5**, the experiment was carried out in DMF while it was performed in CH_2Cl_2 for the more soluble complexes **7** and **9**. The changes in the UV–Vis-NIR spectra upon oxidation of **5** and **7** are shown in Figure 4. The absorption spectra show that the neutral complexes **5** and **7** absorb in the UV–Vis region but not beyond 400 nm. In both cases, upon gradual oxidation, only the spectral signature of the TTF radical cation species at 460 nm and 680 nm is observed for **5** and at 440 nm and 810 nm for **7** with no evidence of intervalence charge-transfer (IVCT) bands at lower energies. Similar evolution of the UV–Vis-NIR spectra were observed for the Pt complex with a shorter linkage, *trans*-[Pt(C≡CMe$_3$TTF)$_2$(PPh$_3$)$_2$] [23].

Concerning the investigation carried out on the complex **9**, the evolution of the spectra upon oxidation is totally different (Figure 5). The neutral complex exhibits absorption bands in the UV–visible range at λ_{max} values of 259, 320 and 400 nm, but not beyond. Gradual oxidation from neutral to mono-oxidized species leads to a diminution of UV visible absorption bands at λ = 320 and 400 nm and the new bands growth at λ = 355, 445, 640 nm and λ = 1300 nm (0.95 eV), the last one being a broad absorption band. Previous studies on the ethyne analogue complex *trans*-[RuCl(C≡CMe$_3$TTF)(dppe)$_2$] have shown a similar evolution of the spectra upon oxidation with the same kind of broad band in the NIR range at 1399 nm (0.88 eV) due to a SOMO–LUMO transition [17]. That is consistent with an electronic communication between the TTF and ruthenium moieties existing in both complexes.

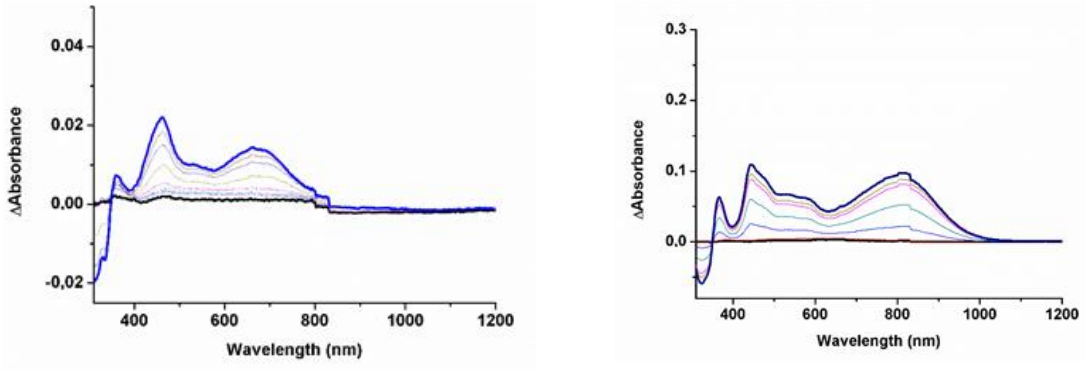

(**a**) (**b**)

Figure 4. Differential UV–Vis-NIR spectra recorded during the oxidation of *trans*-[Hg(C≡CMe_3TTF)$_2$(dppe)$_2$] **5** (**a**) and *trans*-[Pt(C≡C–C≡CMe_3TTF)$_2$(PPh_3)$_2$] **7** (**b**).

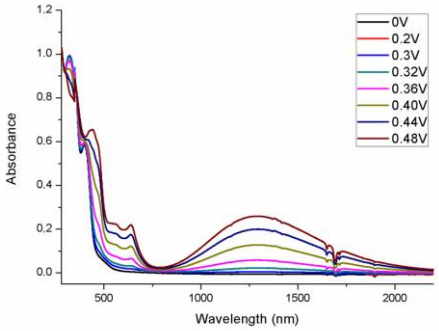

Figure 5. UV–Vis-NIR monitoring of the electrochemical oxidation of *trans*-[RuCl(C≡C–C≡CMe_3TTF)(dppe)$_2$] to the monooxidized complex.

3. Materials and Methods

General Procedures. All the reactions were performed under an argon atmosphere using standard Schlenk techniques. The solvents were purified and dried by standard methods. The *cis*-$RuCl_2$(dppe)$_2$ and trimethylsilylprotected TTF **1** were synthesized according to procedures laid out in the literature [16–18]. NMR spectra were recorded on a AV300III spectrometer (Bruker, Billerica, MA, USA). Chemical shifts were reported in ppm and ^{1}H NMR spectra were referenced to residual $CHCl_3$ (7.26 ppm). ^{31}P NMR spectra were referenced to H_3PO_4. The ^{13}C NMR spectra of complexes *trans*-[Hg(–C≡C–Me_3TTF)$_2$] and *trans*-[Hg(–C≡C–C≡C–Me_3TTF)$_2$] could not be obtained due to their low solubility. Mass spectra were recorded by the Centre Régional de Mesures Physiques de l'Ouest, Rennes. Cyclic voltammetry investigations were carried out on a 10^{-3} M solution containing 0.1 M NBu_4PF_6 as a supporting electrolyte. Voltammograms were recorded at 0.1 V·s^{-1} on a platinum disk electrode. The potentials were measured against the Saturated Calomel Electrode (SCE). The spectroelectrochemical setup was performed in a solution containing NBu_4PF_6 0.2 M, using a Pt grid as the working electrode, a Pt wire as the counter electrode, and SCE reference electrode. A 3600 spectrophotometer (Shimatzu, Kyoto, Japan) was employed to record the UV–Vis-NIR spectra.

3.1. Synthesis of TTF **2**

K_2CO_3 (4.2 mmol, 600 mg) was added to a solution of TTF **1** (0.6 mmol, 250 mg) in tetrahydrofuran/methanol (1/1, 40 mL). After stirring for 30 min, the mixture was extracted with CH_2Cl_2 and then concentrated. A solution of CuI (1.4 mmol, 265 mg) and tetramethylethylenediamine (2 mmol, 0.3 mL) in CH_2Cl_2 (6 mL) was then added to the mixture with additional CH_2Cl_2 (40 mL) and trimethylsilylacetylene (11 mmol, 1.5 mL). After stirring for 3 h, the mixture was extracted with

CH_2Cl_2, and purified by chromatography (SiO_2, CH_2Cl_2/Pentane 1/2) to afford TTF **2** as a red powder in a 95% yield. ^{1}H NMR (300 MHz, $CDCl_3$) δ 2.16 (s, 3H, Me), 1.95 (s, 6H, Me), 0.23 (s, 9H, $SiMe_3$); IR $\nu_{C\equiv C}$ 2185 cm^{-1}, 2097 cm^{-1}; mp = 147 °C [30].

3.2. Synthesis of trans-[Hg(C≡CMe$_3$TTF)$_2$] **5**

$Hg(OAc)_2$ (0.13 mmol, 42 mg) was added to a solution of TTF **3** (0.26 mmol, 70 mg) in dry THF. After stirring under reflux for 12 h, the mixture was filtered off and the precipitate was washed with THF and CH_2Cl_2 to afford the complex *trans*-[Hg(C≡C–Me$_3$TTF)$_2$] **5** as an orange powder in 56% yield. ^{1}H NMR (300 MHz, DMSO) δ 2.13 (s, 6H, Me), 1.94 (s, 12H, Me); ^{1}H NMR (300 MHz, C_5D_5N) δ 2.22 (s, 6H, Me), 1.77 (s, 12H, Me); IR $\nu_{C\equiv C}$ 2141 cm^{-1}; HRMS calcd for $C_{22}H_{18}HgS_8$ [M]$^{+\cdot}$739.8863, found 739.8875.

3.3. Synthesis of trans-[Hg(C≡C–C≡CMe$_3$TTF)$_2$] **6**

$Hg(OAc)_2$ (0.14 mmol, 45 mg) was added to a solution of TTF **4** (0.28 mmol, 83 mg) in dry THF. After stirring under reflux for 12 h, the mixture was filtered off and the precipitate was washed with THF and CH_2Cl_2 to afford the complex *trans*-[Hg(C≡C–C≡CMe$_3$TTF)$_2$] as a light red powder in 30% yield. ^{1}H NMR ^{1}H (300 MHz, C_5D_5N) δ 1.99 (s, 6H, Me), 1.72 (s, 12H, Me); IR $\nu_{C\equiv C}$ 2188 cm^{-1}.

3.4. Synthesis of trans-[Pt(C≡C–C≡CMe$_3$TTF)$_2$(PPh$_3$)$_2$] **7**

TTF **4** (0.17 mmol, 50 mg), *cis*-$PtCl_2(PPh_3)_2$ (0.085 mmol, 67 mg) and CuI (5 mg) were introduced in a Schlenk tube. After 2 h under vacuum, dry CH_2Cl_2 (10 mL) and triethylamine (5 mL) were added. After stirring over 48 h, the mixture was filtered, washed by water and dried under vacuum. The crude product was purified by chromatography (SiO_2, CH_2Cl_2) to afford *trans*-[Pt(C≡C–C≡C–Me$_3$TTF)$_2$(PPh$_3$)$_2$] as a red dark powder in 52% yield. ^{1}H NMR (300 MHz, $CDCl_3$) δ 7.70–7.41 (m, 30 H, H_φ) 1.92 (m, 18H, CH_3); ^{31}P NMR (120 MHz, $CDCl_3$) δ 18.1 (s, 2P); IR $\nu_{C\equiv C}$ 2160 cm^{-1}, 2056 cm^{-1}; HRMS *m*/*z* calcd for $C_{62}H_{48}P_2S_8Pt$ 1305.06449; found 1305.0638.

3.5. Synthesis of trans-[RuCl(C≡C–C≡C–Me$_3$TTF)(dppe)$_2$] **9**

TTF **4** (0.34 mmol, 100 mg), *cis*-$RuCl_2$(dppe)$_2$ (0.33 mmol, 320 mg) and $NaPF_6$ (0.40 mmol, 67 mg) were introduced in a Schlenk tube. After 2 h under vacuum, dry CH_2Cl_2 (40 mL) and triethylamine (1 mmol, 140 µL) were added. After stirring overnight, the mixture was filtered, washed by water and dried under vacuum. The crude product was washed by ether and filtered to afford *trans*-[RuCl(C≡C–C≡C–Me$_3$TTF)(dppe)$_2$] as a brown powder in 30% yield. ^{1}H NMR (300 MHz, $CDCl_3$) δ 7.6–6.9 (m, 40 H, H_φ) 2.66 (s, 8H, CH_2), 2.10 (s, 3H, Me), 1.96 (s, 6H, Me); ^{31}P NMR (120 MHz, $CDCl_3$) δ 47.9 (s, 4P); IR $\nu_{C\equiv C}$ 2134 cm^{-1}, 2011 cm^{-1}; HRMS *m*/*z* calcd for $C_{65}H_{57}ClP_4S_4Ru$ 1226.10202; found 1226.1023.

3.6. Crystallography

Data were collected on an APEXII, Bruker-AXS diffractometer, for complexes **5** and **9**, Mo Kα radiation (λ = 0.71073 Å). The structures were solved by direct methods using the *SIR*97 program [39], and then refined with full-matrix least-square methods based on F^2 (*SHELXL*-97) [40] with the aid of the WINGX program [41]. All non-hydrogen atoms were refined with anisotropic atomic displacement parameters. H-atoms were finally included in their calculated positions. Crystallographic data on X-ray data collection and structure refinements are given in Table 4. The X-ray crystallographic data for structural analysis reported in this article have been deposited in the Cambridge Crystallographic Data Center, under the deposition numbers CCDC 1834591–1834592. These data can be obtained free of charge from the Cambridge Crystallographic Data Center via http://www.ccdc.cam.ac.uk/data_request/cif.

Table 4. Crystalloraphic data for complexes **5** and **9**.

Compound	5	9
Formula	$C_{22}H_{18}HgS_8$, $2C_5H_5N$	$C_{65}H_{57}ClP_4RuS_4$, $2CH_2Cl_2$
FW ($g{\cdot}mol^{-1}$)	897.63	1396.6
Crystal system	triclinic	triclinic
space group	$P\bar{1}$	$P\bar{1}$
a (Å)	8.8323(5)	9.1798(4)
b (Å)	10.0293(5)	12.9853(7)
c (Å)	11.0770(6)	27.0066(14)
α (°)	63.264(2)	77.795(3)
β (°)	73.055(3)	83.777(2)
γ (°)	80.624(2)	80.909(2)
V ($Å^3$)	837.69(8)	3097.6(3)
T(K)	150(2)	150(2)
Z	1	2
D_{calc} ($g{\cdot}cm^{-3}$)	1.779	1.497
μ (mm^{-1})	5.119	0.749
Total refls	11,468	40,676
Uniq. refls.(R_{int})	3813(0.0346)	14,112(0.0949)
Unique refls. ($I > 2s(I)$)	3641	8399
R_1, wR_2	0.0350, 0.0904	0.0783, 0.1977
R_1, wR_2 (all data)	0.0373, 0.0918	0.1298, 0.2281
GoF	1.065	1.071

4. Conclusions

In summary, we have synthesized four new complexes where either two TTFs are connected by an organometallic linkage (M = Hg, Pt) or one TTF is linked through a butadiynyl linker to a $RuCl(dppe)_2$ fragment. These four complexes, *trans*-$[Hg(C{\equiv}CMe_3TTF)_2]$, *trans*-$[Hg(C{\equiv}C{-}C{\equiv}CMe_3TTF)_2]$, *trans*-$[Pt(C{\equiv}C{-}C{\equiv}CMe_3TTF)_2(PPh_3)_2]$ and *trans*-$[RuCl(C{\equiv}C{-}C{\equiv}CMe_3$ $TTF)(dppe)_2]$ complete a series of previously reported metal (Pt, Ru) bis(alkynyl-tetrathiafulvalene) complexes. The electrochemical and spectroelectrochemical investigations carried out on these novel complexes have been analyzed and compared. Cyclic voltammetry experiments allowed us to evaluate the extent of the interaction between the TTFs depending on the nature of the bridging metal (Hg, Pt, Ru) and the length of the conjugated organic linker. No modification of the redox potentials of the TTFs within the mercury complexes has been observed. This indicates that the two TTFs behave as if they were independent. Concerning the platinum complexes, no evidence of electronic communication between the two peripheral TTFs was shown. However, within the platinum complexes, the organometallic fragment through the conjugated linker induces an increase of the electron density on the TTF cores due to the electronic interaction between the metal center and the TTFs. The ruthenium complexes are the only ones where mutual strong electronic interactions between the TTF and the Ru atom have been demonstrated, together with electronic coupling between the two covalently linked TTFs, and the extent of the interaction decreasing with the length of the conjugated bridge. Further investigations on these complexes will be devoted to the elaboration of the oxidized species by electrocrystallization.

Author Contributions: Morgan Auffray and Antoine Vacher performed the experiments; Thierry Roisnel carried out XRD analysis; Dominique Lorcy conceived the project and wrote the paper

Conflicts of Interest: The authors declare no conflict of interest.

References

1. Iyoda, M.; Hasegawa, M.; Miyake, Y. Bi-TTF, bis-TTF and related oligomers. *Chem. Rev.* **2004**, *104*, 5085–5114. [CrossRef] [PubMed]

2. Jeppesen, J.O.; Nielsen, M.B.; Becher, J. Tetrathiafulvalene cyclophanes and cage molecules. *Chem. Rev.* **2004**, *104*, 5115–5131. [CrossRef] [PubMed]
3. Jiang, H.; Mazzanti, V.; Parker, C.R.; Broman, S.L.; Wallberg, J.H.; Luspai, K.; Brincko, A.; Kjaergaard, H.G.; Kadziola, A.; et al. Interactions between tetrathiafulvalene units in dimeric structures—The influence of cyclic cores. *Beilstein J. Org. Chem.* **2015**, *11*, 930–948. [CrossRef] [PubMed]
4. Frasconi, M.; Kikuchi, T.; Cao, D.; Wu, Y.; Liu, W.-G.; Dyar, S.M.; Barin, G.; Sarjeant, A.A.; Stern, C.L.; Carmieli, R.; et al. Mechanical Bonds and Topological Effects in Radical Dimer Stabilization. *J. Am. Chem. Soc.* **2014**, *136*, 11011–11026. [CrossRef] [PubMed]
5. Adam, M.; Müllen, K. Oligomeric tetrathiafulvalenes: Extended donors for increasing the dimensionality of electrical conduction. *Adv. Mater.* **1994**, *6*, 439–459. [CrossRef]
6. Aqad, E.; Becker, J.Y.; Bernstein, J.; Ellern, A.; Khodorkovsky, V.; Shapiro, L. New η-electron donors containing two tetrathiafulvalene units fused to 1,4-dithiine and a conducting charge transfer complex with tetracyanoquinodimethane. *J. Chem. Soc. Chem. Commun.* **1994**, 2775–2776. [CrossRef]
7. Danila, I.; Biaso, F.; Sidorenkova, H.; Geoffroy, M.; Fourmigué, M.; Levillain, E.; Avarvari, N. Rigid bis(tetrathiafulvalenes) doubly bridged by phosphino groups and derivatives: Synthesis and intramolecular mixed valence state. *Organometallics* **2009**, *28*, 3691–3699. [CrossRef]
8. Avarvari, N.; Fourmigué, M. 1,4-Dihydro-1,4-diphosphinine fused with two tétrathiafulvalènes. *Chem. Commun.* **2004**, 2794–2795. [CrossRef] [PubMed]
9. Biaso, F.; Geoffroy, M.; Canadell, E.; Auban-Senzier, P.; Levillain, E.; Fourmigué, M.; Avarvari, N. Intramolecular mixed-valence state through silicon or germanium double bridges in rigid bis(Tetrathiafulvalenes). *Chem. Eur. J.* **2007**, *13*, 5394–5400. [CrossRef] [PubMed]
10. Lorcy, D.; Bellec, N.; Fourmigué, M.; Avarvari, N. Tetrathiafulvalene-based group XV ligands: Synthesis, coordination chemistry and radical cation salts. *Coord. Chem. Rev.* **2009**, *253*, 1398–1438. [CrossRef]
11. Bergkamp, J.J.; Decurtins, S.; Liu, S.-X. Current advances in fused tetrathiafulvalene donor–acceptor systems. *Chem. Soc. Rev.* **2015**, *44*, 863–874. [CrossRef] [PubMed]
12. Vajpayee, V.; Bivaud, S.; Goeb, S.; Croué, V.; Allain, M.; Popp, B.V.; Garci, A.; Therrien, B.; Sallé, M. Electron-rich arene–ruthenium metalla-architectures incorporating tetrapyridyl–tetrathiafulvene donor moieties. *Organometallics* **2014**, *33*, 1651–1658. [CrossRef]
13. Massue, J.; Bellec, N.; Chopin, S.; Levillain, E.; Roisnel, T.; Clérac, R.; Lorcy, D. Electroactive ligands: The first metal complexes of tetrathiafulvenyl−acetylacetonate. *Inorg. Chem.* **2005**, *44*, 8740–8748. [CrossRef] [PubMed]
14. Bellec, N.; Massue, J.; Roisnel, T.; Lorcy, D. Chelating ability of a conjugated redox active tetrathiafulvalenyl-acetylacetonate ligand. *Inorg. Chem. Comm.* **2007**, *10*, 1172–1176. [CrossRef]
15. Liu, W.; Xiong, J.; Wang, Y.; Zhou, X.-H.; Wang, R.; Zuo, J.-L.; You, X.-Z. Syntheses, structures, and properties of tricarbonyl (chloro) rhenium(I) complexes with redox-active tetrathiafulvalene−pyrazole ligands. *Organometallics* **2009**, *28*, 755–762. [CrossRef]
16. Vacher, A.; Barriere, F.; Roisnel, T.; Piekara-Sady, L.; Lorcy, D. Electronically coupled tetrathiafulvalene electrophores across a non-innocent acetylide–ruthenium bridge. *Organometallics* **2011**, *30*, 3570–3578. [CrossRef]
17. Vacher, A.; Barrière, F.; Roisnel, T.; Lorcy, D. Electronic communication between metal–organic electrophores in an organometallic ruthenium–acetylide–tetrathiafulvalene complex. *Chem. Commun.* **2009**, 7200–7202. [CrossRef] [PubMed]
18. Vacher, A.; Barrière, F.; Lorcy, D. Ferrocene and tetrathiafulvalene redox interplay across a bis-acetylide–ruthenium bridge. *Organometallics* **2013**, *32*, 6130–6135. [CrossRef]
19. Nishijo, J.; Judai, K.; Nishi, N. Weak ferromagnetism and strong spin−spin interaction mediated by the mixed-valence ethynyltetrathiafulvalene-type ligand. *Inorg. Chem.* **2011**, *50*, 3464–3470. [CrossRef] [PubMed]
20. Nishijo, J.; Enomoto, M. A Series of weak ferromagnets based on a chromium–acetylide–TTF type complex: Correlation of the structures and magnetic properties and origin of the weak ferromagnetism. *Inorg. Chem.* **2013**, *52*, 13263–13268. [CrossRef] [PubMed]
21. Nishijo, J. Chromium–ethynyltetrathiafulvalene complex based magnetic materials. *Polyhedron* **2013**, *66*, 43–47. [CrossRef]
22. Nishijo, J.; Shima, Y.; Enomoto, M. Synthesis, crystal structures and magnetic properties of new chromium(III)–acetylide–TTF type complexes. *Polyhedron* **2017**, *136*, 35–41. [CrossRef]

23. Vacher, A.; Barrière, F.; Camerel, F.; Bergamini, J.F.; Roisnel, T.; Lorcy, D. *Cis* and *trans*-bis(tetrathiafulvalene-acetylide) platinum(II) complexes: Syntheses, crystal structures, and influence of the ancillary ligands on their electronic properties. *Dalton Trans.* **2013**, *42*, 383–394. [CrossRef] [PubMed]
24. Fourmigué, M.; Huang, Y.-S. Evaluation of the extent of interaction within dimeric tetrathiafulvalenes (TTF) incorporating organometallic -Hg-, -SiMe2-, and -PPh- links. *Organometallics* **1993**, *12*, 797–802. [CrossRef]
25. Buschbeck, R.; Low, P.J.; Lang, H. Homoleptic transition metal acetylides. *Coord. Chem. Rev.* **2011**, *255*, 241–272. [CrossRef]
26. Wong, W.-Y. Mercury alkynyls as versatile templates for new organometallic materials and polymers. *Coord. Chem. Rev.* **2007**, *251*, 2400–2427. [CrossRef]
27. Bruce, M.I.; Halet, J.-F.; Le Guennic, B.; Skelton, B.W.; Smith, M.E.; White, A.H. Preparation and molecular structure of $Hg\{C{\equiv}CC{\equiv}C[Ru(dppe)Cp^*]\}_2$-non linearity in a molecular rod. *Inorg. Chim. Acta* **2003**, *350*, 175–181. [CrossRef]
28. Vacher, A.; Auffray, M.; Barrière, F.; Roisnel, T.; Lorcy, D. Electronic interplay between TTF and extended-TCNQ electrophores along a ruthenium bis(acetylide) linker. *Org. Lett.* **2017**, *19*, 6060–6063. [CrossRef] [PubMed]
29. Lebreton, C.; Touchard, D.; Le Pichon, L.; Daridor, A.; Toupet, L.; Dixneuf, P.H. Mono- and bis-alkynyl ruthenium (II) complexes containing the ferrocenyl moiety; crystal structure of *trans*-$[Ru(C{\equiv}CC_5H_4FeC_5H_5)_2(Ph_2PCH_2CH_2PPh_2)]$ and electrochemical studies. *Inorg. Chim. Acta* **1998**, *272*, 18–196. [CrossRef]
30. Yzambart, G.; Fabre, B.; Camerel, F.; Roisnel, T.; Lorcy, D. Controlled grafting of tetrathiafulvalene (TTF) containing diacetylenic units on hydrogen-terminated silicon surfaces: From redox-active TTF monolayer to polymer films. *J. Phys. Chem. C* **2012**, *116*, 12093–12102. [CrossRef]
31. Jones, G.E.; Kendrick, D.A.; Holmes, A.B. 1,4-Bis(trimethylsilyl)buta-1,3-diyne. *Org. Synth.* **1987**, *65*, 52. [CrossRef]
32. Basseti, M.; Floris, B.; Illuminati, G. The reaction of ethynylferrocene with mercuric acetate. *Organometallics* **1985**, *4*, 617–623. [CrossRef]
33. Dietrich, S.; Mansilla, N.; Hildebrandt, A.; Wetzold, N.; Rheinwald, G. Alkynyl Ti–M complexes with M=Cd and Hg: Synthesis, characterization, and reaction chemistry. *J. Organomet. Chem.* **2011**, *696*, 2491–2498. [CrossRef]
34. Dewhurst, R.D.; Hill, A.F.; Smith, M.K. Hazards associated with bis(alkynyl)mercurials. *Organometallics* **2006**, *25*, 2388–2389. [CrossRef]
35. Sadowy, A.L.; Ferguson, M.J.; McDonald, R.; Tykwinski, R.R. Chiral *cis*-platinum acetylide complexes via diphosphine ligand exchange: Effect of the ligand. *Organometallics* **2008**, *27*, 6321–6325. [CrossRef]
36. Colbert, M.C.B.; Lewis, J.; Long, N.J.; Raithby, P.R.; White, A.J.P.; Williams, D.J. Synthetic, structural, electrochemical and electronic characterisation of heterobimetallic bis(acetylide) ferrocene complexes. *J. Chem. Soc. Dalton Trans.* **1997**, 99–104. [CrossRef]
37. Miyazaki, A.; Ogyu, Y.; Justaud, F.; Ouahab, L.; Cauchy, T.; Halet, J.-F.; Lapinte, C. Synthesis, Molecular Structure, Properties, and Electronic Structures of $[Cp^*(dppe)FeC{\equiv}C{-}TTFMe_3][PF_6]_n$ (n = 0, 1): Electronic Coupling between the Inorganic and Organic Electrophores. *Organonetallics* **2010**, *29*, 4628–4638. [CrossRef]
38. Justaud, F.; Gendron, F.; Ogyu, Y.; Kumamoto, Y.; Miyazaki, A.; Ouahab, L.; Costuas, K.; Halet, J.-F.; Lapinte, C. Hybrid Molecular Systems Containing Tetrathiafulvalene and Iron-Alkynyl Electrophores: Five-Component Functional Molecules Obtained from C–H Bond Activation. *Chem. Eur. J.* **2013**, *19*, 5742–5757. [CrossRef] [PubMed]
39. Altomare, A.; Burla, M.C.; Camalli, M.; Cascarano, G.; Giacovazzo, C.; Guagliardi, A.; Moliterni, A.G.G.; Polidori, G.; Spagna, R.J. *SIR*97: A new tool for crystal structure determination and refinement. *J. Appl. Cryst.* **1999**, *32*, 115–119. [CrossRef]
40. Sheldrick, G.M. A short history of *SHELX*. *Acta Cryst.* **2008**, *A64*, 112–122. [CrossRef] [PubMed]
41. Farrugia, L.J. WinGX and ORTEP for Windows: An update. *J. Appl. Cryst.* **2012**, *45*, 849–854. [CrossRef]